



# Potential choline kinase inhibitors: A molecular modeling study of *bis*-quinolinium compounds<sup>☆</sup>

P. Srivani, G. Narahari Sastry<sup>\*</sup>

Molecular Modeling Group, Organic Chemical Sciences, Indian Institute of Chemical Technology, Tarnaka, Hyderabad 500007, India

## ARTICLE INFO

### Article history:

Received 15 August 2008

Received in revised form 10 October 2008

Accepted 27 October 2008

Available online 6 December 2008

### Keywords:

*bis*-Quinolinium derivatives

Choline kinase

Docking

QSAR

CoMFA

CoMSIA

Phosphocholine

Molecular modeling

## ABSTRACT

Choline kinase (ChoK) is reported to involve in cell signaling pathways and cell growth by regulating the intermediate, phosphocholine (PCho), which is the first step to biosynthesis a membrane phospholipid, phosphatidylcholine. The PCho levels are overexpressed due to elevated activation of the protein under carcinogenesis conditions. ChoK has thus evolved as a novel target for various cancers and a range of compounds has been reported in this course as potent ChoK inhibitors. However, not much information is known about the binding site of the inhibitors. Therefore, we ventured to unravel the possible binding site of 39 *bis*-quinolinium inhibitors from which the structural requirement for better protein–ligand complex was delved. Molecular docking and 3D-QSAR studies namely comparative molecular field analysis (CoMFA) and comparative molecular similarity indices analysis (CoMSIA) were performed on the series. The knowledge of the active site was obtained from the site id search and molcad surface calculations of Sybyl, which was further considered for docking studies. In 3D-QSAR, the best predictions were obtained from the model where 29 compounds were considered in the training set and remaining 10 in the test set. The best CoMFA statistics were obtained with  $r^2$  of 0.99 and  $q^2$  of 0.81 while, CoMSIA was resulted with  $r^2$  of 0.98 and  $q^2$  of 0.77. A comparative analysis was done with the resulted 3D-QSAR maps and the docked poses by overlaying the maps on the active site residues. Since, there is no reported ligand co-crystallized structure of ChoK the present study provides valuable clues on the binding conformation of the ligand and its interactions with the active site.

© 2008 Elsevier Inc. All rights reserved.

## 1. Introduction

Choline kinase (ChoK) is a phosphotransferase enzyme present in the cytosol and known to involve in cell signaling pathways by regulating the synthesis of phosphocholine (PCho) from choline (I). The generation of PCho is considered to be one of the crucial steps in regulating growth factor stimulated cell proliferation, malignant transformation, invasion, metastasis besides inducing the DNA-synthesis [1]. It has been observed that during the tumor formation the phospholipid metabolism is being altered, which consequently leads to the overexpression of PCho [1,2]. The overexpression of PCho is associated with the higher activation of ChoK and it has been reported that various growth factors namely, platelet-derived, epidermal, insulin dependent and vascular endothelial growth factors enhances the ChoK activity during the tumor production [2,3]. Notably, Ras signaling pathway through its two well-known effectors, Ral-GDS and PI3K produces essentially the

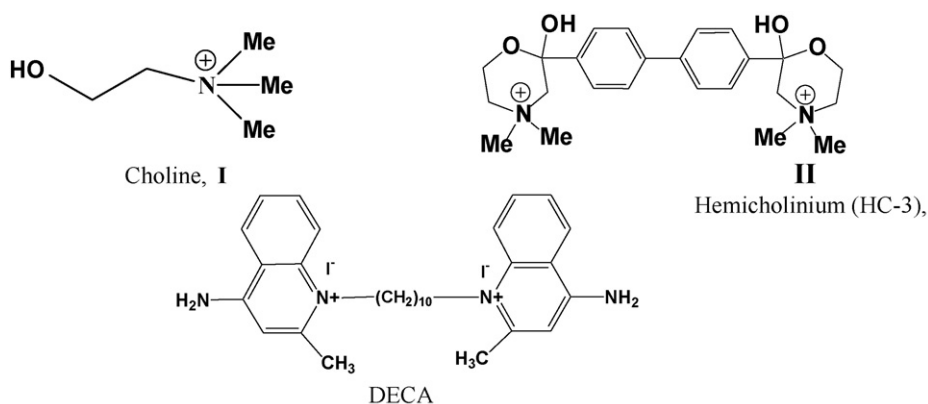
same effect of enhancing the ChoK activity during the tumor formation [4]. Due to its vital role in cell division as well as in tumor formation, ChoK has emerged as a potential target for various cancers particularly for *ras* induced carcinogenesis.

The new cancer therapies that are developed based on *ras* signaling pathway have appeared to be less toxic than the conventional chemotherapies [1,3,5]. Thus, the last 6–7 years have witnessed a frantic activity in the synthesis and analysis of a range of ChoK inhibitors [6–13]. Most of these inhibitors are synthesized by taking the basic skeleton of choline uptake inhibitor, hemicholinium (HC-3, II) (Scheme 1). The HC-3, which is being used from three decades, is a potent competitive inhibitor of the high affinity choline transport system [14]. The strong evidences have shown that II inhibits the effects of growth factors on DNA-synthesis [15–17]. But its use was restricted because of unavoidable side effects like toxic respiratory paralysis effect [3,18]. Therefore, II structure has taken as a template to propose new analogues with devoid of side effects, and attempts to obtain new chemical entities through computational methods [19]. By replacing the hemiketal ring of II with different groups like, pyridinium (III), quinolinium (IV) and isoquinolinium (V) rings various derivatives have been generated in last five years [6–14].

<sup>☆</sup> IICT communication no: 051019.

<sup>\*</sup> Corresponding author. Tel.: +91 40 27160512; fax: +91 40 27160512.

E-mail address: [gnsastry@iict.res.in](mailto:gnsastry@iict.res.in) (G.N. Sastry).

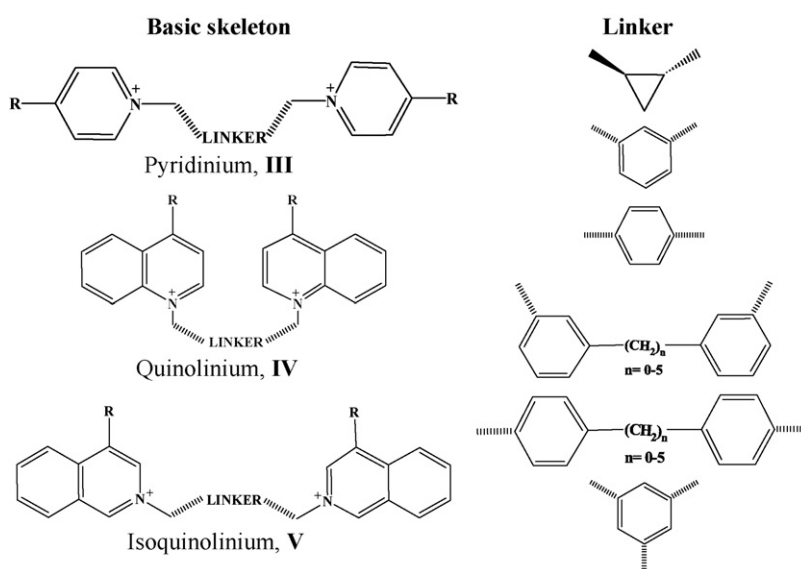


**Scheme 1.** Structures of choline (**I**) and inhibitors, hemicholinium (**II**), which is the basic skeleton for all ChoK inhibitors and DECA, inhibitor for protein kinase C and K<sup>+</sup> channels.

A series of compounds namely *bis*-pyridiniums, -quinoliniums, -isoquinoliniums, cyclopanes, etc. (**Scheme 2**) have been reported as active ChoK inhibitors [9,10,12,14]. The uniqueness of these compounds is that they possess two cationic heads (**III**, **IV**, **V**, etc.) connected through a linker. The cationic moiety of these analogues is maintained to resemble the positive nitrogen of substrate **I**, which shows cation- $\pi$  interactions with aromatic residues (Trp420 and Trp423) of the active site. The inhibitors are assumed to bind to two specific pockets [20] of which choline binding site is the one and no clue is known about the second. The appealing feature of the protein is presence of two known active sites where ATP and choline are expected to bind. The second pocket of the inhibitor is perhaps not the ATP site because the environment of the ATP binding site is completely different from the choline site wherein the environment is suitable to accommodate the positive charge. In addition, the choline binding site is mostly fabricated with aromatic residues to stabilize the positive charge of the nitrogen (N<sup>+</sup>) of **I** through cation- $\pi$  interactions (**Fig. 1**). The density of aromatic residues is more around the choline site i.e. out of 47 residues of the protein, 36 residues are located only in C-terminal domain so as to stabilize the positive charge of **I**. Moreover, the residues which have direct interactions with **I** are stabilized by adjacent aromatic residues, which are not in direct contact with choline, through  $\pi$ - $\pi$  stacking (**Fig. 1**). Thus, all the ChoK inhibitors those are reported so far have the N<sup>+</sup> ion. The cation- $\pi$  interactions which are ubiquitous in nature

[21] are known to effect the neighboring non-covalent interactions significantly [22].

Support for the foregoing discussion has also achieved from other choline binding proteins. Besides acts as a substrate to ChoK, **I** also acts as a precursor as well as a metabolite in the synthesis and degradation of neurotransmitter, acetylcholine (ACh). The degradation step is catalyzed by acetylcholinesterase (AChE) enzyme, which has a narrow 20 Å deep active site gorge wherein the bottom and opening regions are known as catalytic and peripheral sites, respectively [23]. Bivalent ligand strategy has recently been developed to simultaneously target both the sites. Two tryptophan residues each were reported to interact with two azepane rings of the bivalent inhibitors through cation- $\pi$  and hydrophobic interactions in both the sites [23c]. This bivalent strategy has increased the selectivity 10,000-fold towards AChE over butyryl cholinesterase (BChE) [23c]. Another example is from a non-choline protein that is involved in cellular signaling pathways, protein kinase C (PKC), which is a potent antitumor agent in many animal models [24]. A well-known drug, DECA (dequalinium – quinolinium 1,1' (1,10-decanediyl) *bis*(4-amino-2-methyldiiodide)) has been studied as a potent antitumor agent that recognizes several isoforms of PKC *in vitro* (IC<sub>50</sub> = 10–14  $\mu$ M) and *in vivo*. It was hypothesized that the two aromatic moieties of DECA inhibit PKC $\alpha$  activity by coincident contact with two nonoverlapping target sites in the catalytic domain. The linker that is



**Scheme 2.** Basic skeleton of various *bis*-quaternary heterocyclic inhibitors of ChoK along with different linkers are displayed.

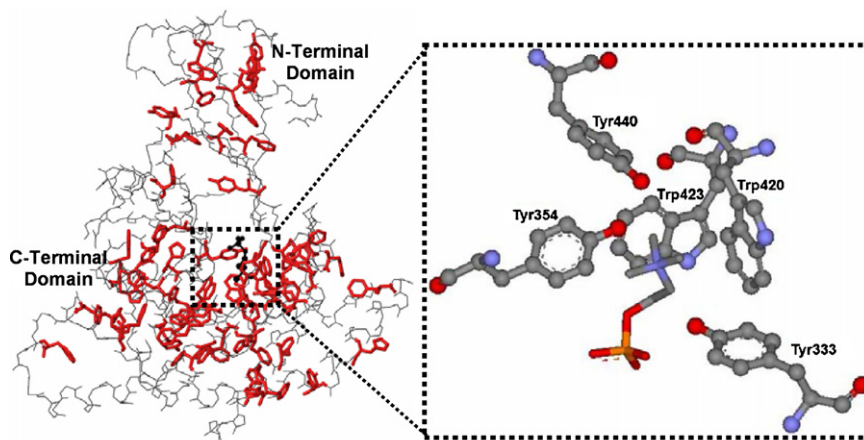


**Fig. 1.** Distribution of aromatic residues (Trp, Tyr and Phe), which are displayed in red capped sticks over the choline kinase protein (2CKQ). The density of aromatic residues is more around the PCho substrate i.e. out of 47 residues, 36 residues are located only in C-terminal domain so as to stabilize the positive charge of the choline and also the residues which have direct interactions with choline are stabilized by adjacent aromatic residues, which are not in direct contact with choline, through  $\pi$ - $\pi$  stacking. The five important aromatic residues that show direct interactions with the PCho are highlighted in the right side image.

connecting the two moieties lies in between these two sites. The sites of interaction in the regulatory and catalytic domains are independent of each other and that the site at which DECA produces inhibition of catalytic activity lies exclusively in the catalytic domain.

Taking the choline as well as inhibitor binding mode similarity of the two proteins into account one can anticipate a similar binding mechanism for ChoK inhibitors. It is not very surprising to find the similarity as it has previously been reported [25] that the architecture of ChoK is similar to eukaryotic protein kinases and bacterial aminoglycoside phosphotransferase.

We have previously reported a comprehensive QSAR study on *bis*-pyridinium analogues [26a]. Human ChoK tertiary structure was not reported at that point in time therefore ligand based approach like QSAR could only be applied on the inhibitors. The report of tertiary structure in the subsequent year facilitated the probes of inhibitor binding mode. Thus, we took a series of 39 *bis*-quinolinium analogues [10] in order to find out the essential structural features towards ChoK inhibitory activity. Following earlier studies of computer aided drug design tools we employed both structure and analog based approaches together for the current problem [26]. We test the possibility of building a comprehensive 3D-QSAR model by means of CoMFA and CoMSIA techniques. The models are further used to deduce the comple-

mentary protein environment for ligand interactions. This in turn evaluated with the structure based approach like docking.

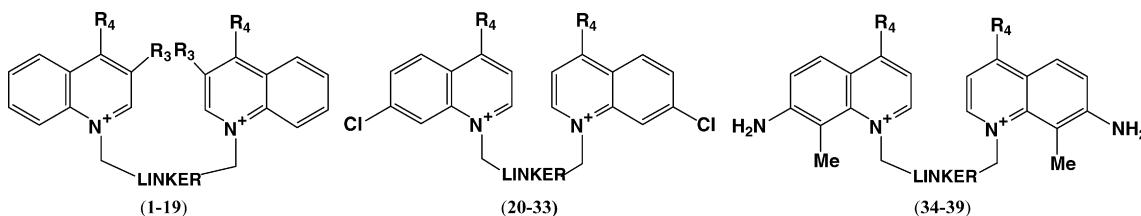
The information about the ChoK tertiary structure is skimpy until Peisach et al. had reported the first crystal structure of ChoK from the source *Caenorhabditis elegans* [25]. The reported structure is an uncomplexed protein with devoid of co-factor and substrate. Following mutational studies and various sequence analysis studies have provided the information regarding the location of ATP and choline binding sites [27]. Recently, Malito et al. had reported three human choline kinase proteins, the *apo* protein and two structures bound with ADP and PCho [28]. Lack of ChoK complex with inhibitor has become a sticking point to further understand the protein–ligand interactions. So, we have taken the reported crystal structures of human ChoK and subjected for active site search. The active site information thus obtained is further used to find out the protein–ligand interactions using different docking protocols.

## 2. Computational details

### 2.1. Data set for analysis

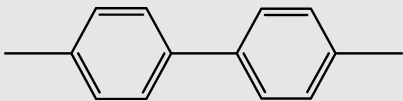
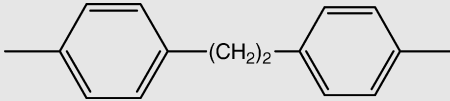
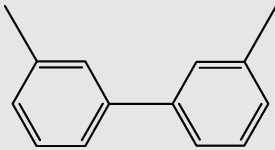
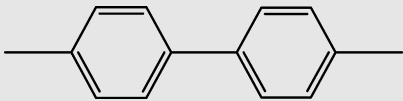
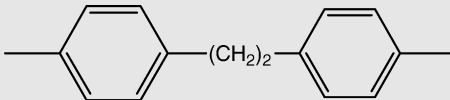
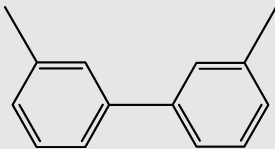
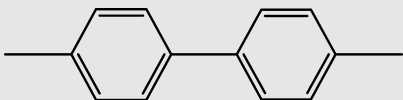
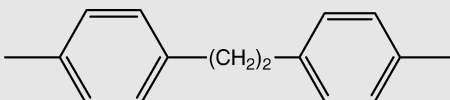
For the present study, a set of 39 *bis*-quinolinium analogues (Table 1) has been taken from the literature [10]. The activities are

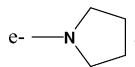
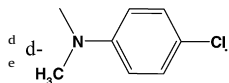
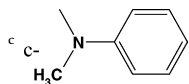
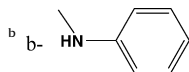
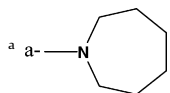
**Table 1**  
The series of *bis*-quinolinium analogs and their activities



Compound number	Linker	R <sub>3</sub>	R <sub>4</sub>	IC <sub>50</sub> (μM)
1		H	-NH <sub>2</sub>	1.20
2		Me	-NH <sub>2</sub>	11.09
3		H	-N(CH <sub>3</sub> ) <sub>2</sub>	4.40
4		H	Perhydroazepino <sup>a</sup>	0.50
5		H	Anilino <sup>b</sup>	1.30
6		H	N-Methylanilino <sup>c</sup>	0.40
7		H	4-Chloro-N-methylanilino <sup>d</sup>	2.10

Table 1 (Continued)

Compound number	Linker	R <sub>3</sub>	R <sub>4</sub>	IC <sub>50</sub> (μM)
8		H	Amino	81.10
9		H	Dimethylamino	39.70
10		H	Perhydroazepino <sup>a</sup>	2.20
11		H	Anilino <sup>b</sup>	17.80
12		H	N-Methylanilino <sup>c</sup>	3.00
13		H	4-Chloro-N-methylanilino <sup>d</sup>	2.00
14		H	Amino	80.00
15		H	Dimethylamino	10.20
16		H	Perhydroazepino <sup>a</sup>	0.60
17		H	Anilino <sup>b</sup>	2.30
18		H	N-Methylanilino <sup>c</sup>	1.40
19		H	4-Chloro-N-methylanilino <sup>d</sup>	4.80
20			Amino	20.60
21			Dimethylamino	9.60
22			Pyrrolidino <sup>e</sup>	1.20
23			N-Methylanilino <sup>c</sup>	3.10
24			4-Chloro-N-methylanilino <sup>d</sup>	5.70
25			Amino	63.30
26			Dimethylamino	20.60
27			Pyrrolidino <sup>e</sup>	19.80
28			N-Methylanilino <sup>c</sup>	11.40
29			4-Chloro-N-methylanilino <sup>d</sup>	11.40
30			Dimethylamino	9.00
31			Pyrrolidino <sup>e</sup>	1.00
32			N-Methylanilino <sup>c</sup>	3.50
33			4-Chloro-N-methylanilino <sup>d</sup>	5.70
34				56.80
35			N-Methylanilino <sup>c</sup>	
			4-Chloro-N-Methylanilino <sup>d</sup>	147.00
36			N-Methylanilino <sup>c</sup>	96.10
37			4-Chloro-N-methylanilino <sup>d</sup>	46.10
38			N-Methylanilino <sup>c</sup>	133.00
39			4-Chloro-N-methylanilino <sup>d</sup>	57.50



distributed within a range of 0.40–147  $\mu\text{M}$ . The inhibitor activities ( $\text{IC}_{50}$ ) against human ChoK was converted into  $\text{pIC}_{50}$  according to the formula  $\text{pIC}_{50} = -\log(\text{IC}_{50})$ .

## 2.2. Molecular modeling

Three different software packages, Sybyl 6.9, GOLD 3.2, and Schrodinger suite 2007 have been used for the purpose of molecule preparation, active site search and docking [29–31]. Protein and ligands were prepared in the respective software separately. While for 3D-QSAR all the ligands were prepared using Sybyl 6.9 version. The conformation of the ligands is perhaps an important and most crucial step for a 3D-QSAR study. In absence of experimental details concerning the ‘bio-active’ conformation of the ligand assigning the correct conformation is a difficult task. In the present study, a keen analysis of the protein active site has provided a few possibilities of how ChoK inhibitors can bind in the protein active site and what would be the inhibitor binding mode. The two-quinolinium moieties of the ligand may bind to two different sites and the linker region is most likely to locate in between. The ligands were considered accordingly, in the above-discussed manner, and optimized in order to get the best statistical fits. MMFF94 force field and MMFF94 partial atomic charges were employed with distance dependent dielectric constant and Powell’s conjugate gradient method was used until a convergence criterion of 0.001 kcal/mol was reached.

Besides the conformation of the ligand, alignment is another decisive step in 3D-QSAR studies, because, choosing the correct template for alignment will furnish a statistically reliable model. Hence, we have attempted quiet a few models with various templates (linker, phenyl ring and benzyl quinolinium) and the one with the benzyl quinolinium moiety was resulted with considerably good results (Table 2). For the purpose of analysis all the dataset molecules were categorized in to three sets, Set A, B and C,

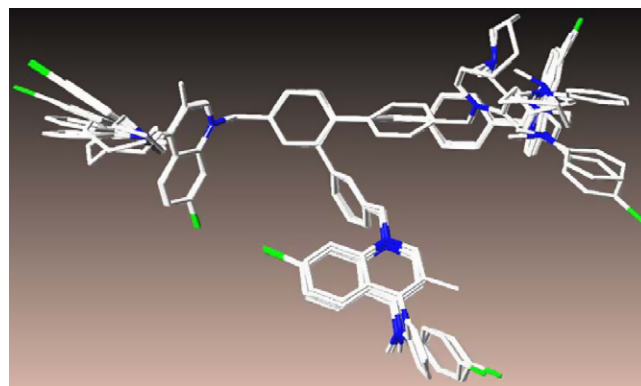


Fig. 2. Alignment of the dataset molecules using database alignment protocol.

based on three structurally different linkers. Initially, the molecules in each individual sets were aligned based on the linker using atom fit module of Sybyl then each set is overlaid on other sets by taking the benzyl quinolinium ring as a template using database alignment option (Fig. 2).

## 2.3. Generation of CoMFA and CoMSIA fields

The steric and electrostatic potential fields for CoMFA were calculated at each lattice intersection of a regularly spaced grid of 2.0 Å in all the three dimensions within the defined region. The steric and electrostatic fields were calculated using Lennard-Jones 6–12 and columbic terms, respectively. A distance dependent dielectric constant of 1.0 was used. A sp<sup>3</sup> carbon atom with a radius of 1.52 Å and +1.0 charge was served as the probe atom to calculate steric and electrostatic fields. The steric and electrostatic contributions were truncated to  $\pm 30$  kcal/mol, and electrostatic contributions were ignored at lattice intersections with maximum steric interactions. The CoMFA steric and electrostatic fields generated were scaled by CoMFA standard option.

Five CoMSIA fields (steric, electrostatic, hydrophobic, hydrogen bond donor, and hydrogen bond acceptor) were calculated using the probe atom. CoMSIA fields were derived according to Klebe et al. with a grid spacing of 2 Å employing a C<sup>+</sup> probe atom with a radius of 1.0 Å [32]. A Gaussian type distance dependent function was used between the grid point  $q$  and each atom  $i$  of the molecule. The default attenuation factor ( $\alpha$ ) of 0.3 was used. In CoMSIA, the steric indices are related to the third power of the atomic radii, the electrostatic descriptors are derived from atomic partial charges, the hydrophobic fields are derived from atom-based parameters developed by Viswanadhan et al., and the hydrogen bond donor and acceptor indices are obtained by a rule-based method derived from experimental values [33–35].

## 2.4. Partial-least-square (PLS) analysis

PLS analysis was used to derive a linear correlation between the 3D-fields (independent variables) and the inhibitory activity values (dependent variables) [36]. The cross-validation analysis was performed using leave-one-out (LOO) method that returns the optimum number of components for which it has maximum cross-validated  $r^2$  ( $q^2$ ) and minimum standard error of prediction (SEP). In order to overcome the over-fitting problem, no-validation run was performed using the same optimum number of components that resulted from the cross-validation run. Further to assess the robustness and statistical confidence of the derived models, bootstrapping analysis ( $r_{bs}^2$ ) for 100 runs and cross-validation ( $r_{cv}^2$ ) with 10 groups for 50 runs were performed [36–38].

Table 2  
Statistics of CoMFA and CoMSIA models.

Parameter	CoMFA	CoMSIA			
		Model-I <sup>a</sup>	Model-II <sup>b</sup>	Model-III <sup>c</sup>	Model-IV <sup>d</sup>
$r^2$	0.99	0.98	0.97	0.94	0.96
$q^2$	0.81	0.77	0.81	0.69	0.73
SEE <sup>e</sup>	0.08	0.13	0.14	0.22	0.18
SEP <sup>f</sup>	0.38	0.43	0.38	0.49	0.46
$N^g$	6	8	6	7	7
F-value	431.63	120.5	134.33	46.27	71.05
Steric	66.3	21.1	27.5	31.9	–
Electrostatic	33.7	18.3	27.2	32.8	–
Hydrophobic	–	31.6	45.3	–	60.5
Acceptor	–	0.0	–	0.00	0.00
Donor	–	29.0	–	35.2	39.5
PRESS <sup>h</sup>	2.93	–	–	–	–
Cross-validated $r^2$	0.75 <sup>i</sup>	–	–	–	–
	0.65 <sup>j</sup>	–	–	–	–
Bootstrapping					
$r_{bs}^2$		0.99	–	–	–
SD <sup>k</sup>		0.002	–	–	–

<sup>a</sup> Using S, E, H, D, A CoMSIA fields.

<sup>b</sup> Using S, E, H CoMSIA fields.

<sup>c</sup> Using S, E, D, A; CoMSIA fields.

<sup>d</sup> Using H, D, A CoMSIA fields.

<sup>e</sup> Standard error of estimate.

<sup>f</sup> Standard error of prediction.

<sup>g</sup> Number of components.

<sup>h</sup> Predicted residual sum of squares for test set.

<sup>i</sup> Cross-validation run with 10 groups.

<sup>j</sup> Cross-validation run with 5 groups.

<sup>k</sup> Standard deviation.



Bootstrapping involves the generation of many new data sets from original data set and is obtained by randomly choosing samples from the original data set. The statistical calculation is performed on each of these bootstrapping samplings. The difference between the parameters calculated from the original data set and the average of the parameters calculated from the many bootstrapping samplings is a measure of the bias of the original calculations. The entire cross-validated results were analyzed considering the fact that a value of  $q^2$  above 0.3 indicates that probability of chance correlation is less than 5%. Equal weights were assigned to steric and electrostatic fields using CoMFA-standard scaling option. To speed up the analysis and to reduce the noise, a minimum filter value ( $\sigma$ ) of 2.00 kcal/mol was used. To validate the derived CoMFA and CoMSIA models, biological activities of a test set were predicted.

### 2.5. Active site search and docking studies

All software tools that were mentioned above have been adopted for active site search and for docking studies. The four reported crystal structures of ChOK were downloaded from PDB (Id: 1NW1, 2CKO, 2CKP and 2CKQ). These are homo dimers of chain A and B either having a co crystal of ADP (2CKP) or PCho (2CKQ) or without any substrate (1NW1 and 2CKO).

Initially, for the purpose of active site search, all the water molecules were deleted and the dimer was submitted for Site ID search in Sybyl. Site ID will provide the potential binding sites in a protein using a grid-based flood filled solvation technique [39]. Flood fill algorithm isolates and displays the cavity like binding regions by using solvent molecules. For each solvent molecule in the pocket all atoms in the protein lying within a specified distance of 3 Å were considered. The union of all such atoms was considered as active site where the solvent accessible atoms were colored as red and the remaining cavity atoms belonging to the residues were colored as yellow.

For GOLD docking, all four protein structures were prepared using Sybyl by taking only chain A. All the water molecules were deleted from the crystal structure and all polar and non-polar hydrogens were added. The Kollmann\_all partial atomic charges were assigned followed by the minimization protocol using Tripos force field by aggregating the non-hydrogens for 100 iterations. Then the optimized protein is further considered for docking studies. While for Schrodinger, Protein Preparation Wizard was used to prepare the proteins by taking chain A after adding the hydrogens with default settings. Ligands were submitted for LigPrep module which will generate a range of ionization states that are populated in a given pH range i.e.  $\pm 2$  of 7.4 pH.

The information that was obtained from the active site search as well as from the literature suggested that the region surrounding the choline site is probably the inhibitor binding site. Hence, 15 Å radius from the side chain oxygen atom of Asp306 for 2CKO, 2CKP and 2CKQ proteins and the corresponding residue of 1NW1 was taken to define the active site in GOLD and rest of the settings were taken default. While for Schrodinger, the two modes of docking simple precision (SP) and extra precision (XP) of 'Glide' module was used. The grid was generated by picking the PCho ligand (for 2CKQ) with 10 Å box length ( $x = -20.80$ ,  $y = 32.57$  and  $z = -15.37$ ) and the same coordinates were taken for 1NW1, 2CKP and 2CKO proteins. The default SP docking settings were used and the conformations that have been obtained from SP were used as input for XP.

All docking studies were repeated for two times to get consistent results and also to average out the protein–ligand contacts. The best-docked conformations in each of the cases were taken for further analysis.

## 3. Results and discussion

The dataset was divided into three sets based on type of the linker, Set A (1–7, 20–24, 34 and 35), Set B (8–13, 25–29, 36 and 37) and Set C (14–19, 30–33, 38 and 39).

### 3.1. CoMFA

CoMFA model was generated with a series of 39 compounds out of which 29 were considered as the training set and remaining 10 compounds (1, 10, 12, 14, 15, 23, 25, 26, 29 and 33) in the test set. The CoMFA model was resulted with  $r^2$  of 0.99,  $q^2$  of 0.81 with a PRESS value of 2.93. The resulted group cross-validated  $r^2$  was 0.75 and 0.65 with 10 and 5 groups, respectively. The bootstrapping was resulted with  $r_{bs}^2$  of 0.99, which suggest that the CoMFA model was not based on a chance correlation. The contour plot obtained from the model was representation of the lattice points where differences in field values are strongly associated with the activity. The contour maps were generated as scalar products of coefficients and standard deviation associated with each CoMFA column. The CoMFA steric interactions were represented by green (g) and yellow (y) colored contours while electrostatic interactions were represented by red (r) and blue (b) colored contours. The bulky substituents are favored in green regions and unfavored in yellow regions. The increase in positive charge is favored in blue regions and the increase in negative charge is favored in red regions.

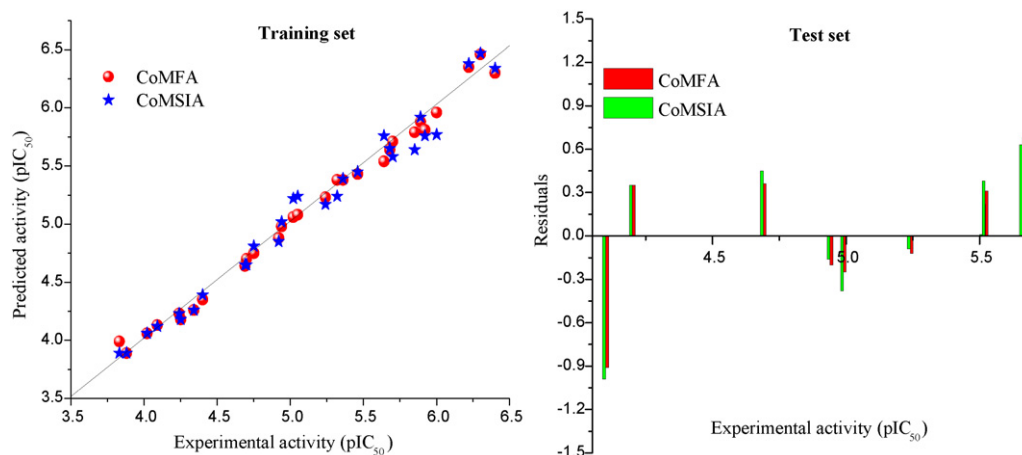
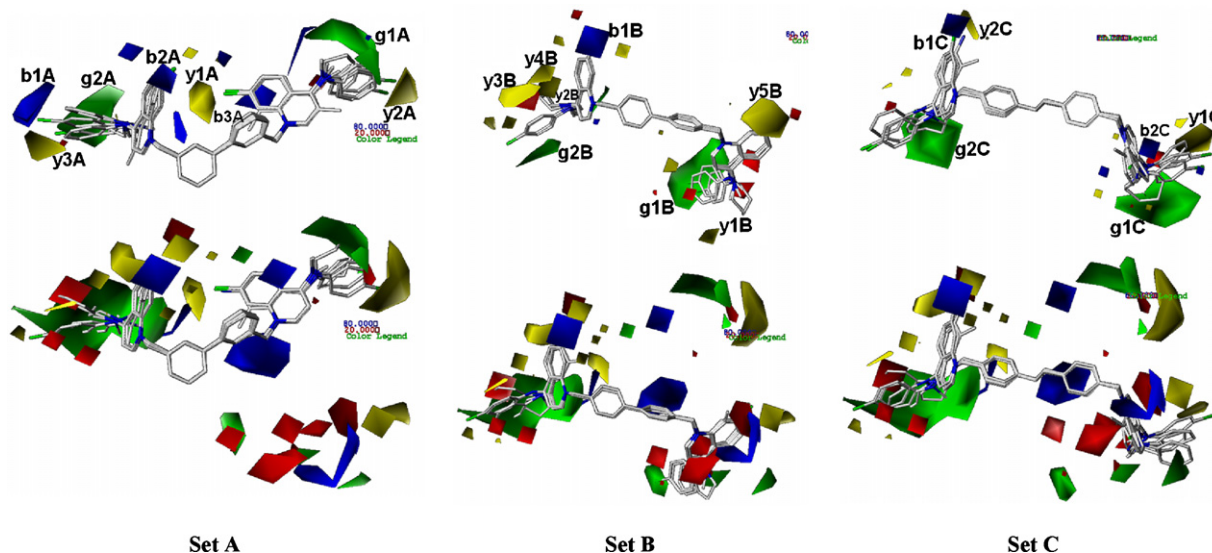


Fig. 3. Plot of actual vs. predicted biological activities for the training and test sets for CoMFA and CoMSIA models.



**Fig. 4.** CoMFA steric and electrostatic contour maps resulted for the dataset. The compounds with different linkers are displayed in the figure. For clarity the maps are only displayed for individual sets. Green (g) contour indicates where bulky group increases the activity whereas yellow (y) contour indicates region where bulky group decreases the activity. Blue (b) contour indicates region where positive charge increases the activity while red (r) contour indicates region where negative charge increases the activity. For the purpose of analysis all the CoMFA maps are named according to the properties (g, y, b and y) and corresponding sets (A, B and C).

### 3.2. CoMSIA

The CoMSIA was obtained by using the same structural alignment, training set and test set that was used for CoMFA but with different combinations of steric, electrostatic, hydrophobic and hydrogen bonding fields. The one model with combination of steric, electrostatic, hydrophobic and hydrogen bond fields gave statistically significant results  $r^2$  of 0.98 and  $q^2$  value of 0.77. The steric contours of CoMSIA, green indicate sterically favorable regions while yellow contours indicate sterically unfavorable regions. In the electrostatic contours, the introduction of electronegative substituents in red regions may increase the affinity while in blue regions decrease the affinity. In hydrophobic contours, orange (o) region favors hydrophobic groups while white (w) region favors hydrophilic groups. In

hydrogen bond donor contours the cyan (c) color is favorable for biological activity and purple (p) color is unfavorable.

The QSAR statistics are given in Table 2. The CoMFA and CoMSIA plots of actual vs. predicted biological activities of the training set and test set are displayed in Fig. 3. The 3D-QSAR contour maps revealing the contribution of CoMFA and CoMSIA fields are shown in Figs. 4 and 5. The compounds with different linkers are displayed in the figures.

For the purpose of analysis the 3D maps were given names for example, green maps were named as g1, g2 and so on and analysis was written sets (A, B and C) viz. (Figs. 4 and 5).

#### 3.2.1. Set A

Two sterically favorable (g1A and g2A) and two unfavorable (y1A and y2A) maps were observed whereas three blue contours

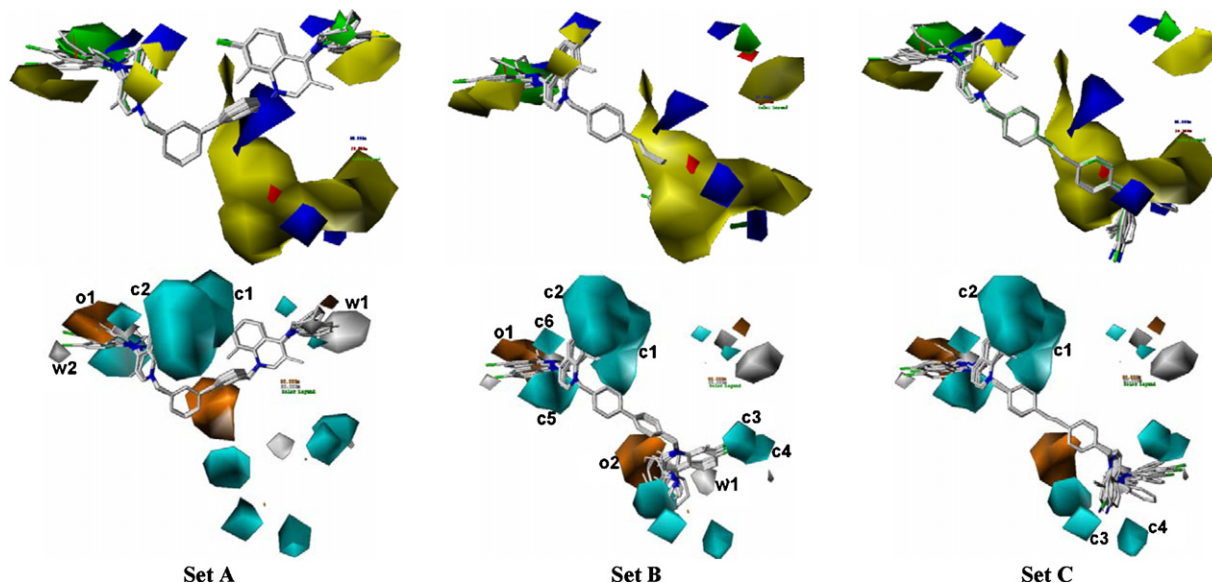


**Fig. 5.** CoMSIA steric, electrostatic, hydrophobic and donor maps for the dataset. The compounds with different linkers are displayed in the figure. The steric (green and yellow) and electrostatic (blue and red) properties are similar to that of CoMFA (Fig. 4). The orange (o) and white (w) colors represent favorable and unfavorable hydrophobic regions, respectively whereas cyan (c) represents for hydrogen bond donor regions. For the purpose of analysis the CoMSIA maps are named according to the properties (o, w and c).

(b1A, b2A and b3A) and no considerable red contour were present (Fig. 4). The g1A and g2A corresponds to R<sub>4</sub> substitution where steric groups/interactions play an important role for the activity. In Set A, the perhydroazepino (**4**), *N*-methylanilino (**6**, **23** and **34**) and pyrrolidino substituents (**22**) have shown good activities comparably to their congeners. The 4-chloro-*N*-methylanilino group is responsible for y3A and y2A. Interestingly, when a model was generated without all 4-chloro-*N*-methylanilino compounds (**7**, **24** and **35**), the two maps (y3A and y2A) were disappeared. The y1A map was resulted from the chloro substitution at 7th position of quinolinium ring particularly for **20** and **21**. While, the b1A was originated from the chloro substitution of 4-chloro-*N*-methylanilino analogues (**7**, **24** and **35**) and a model devoid of these three molecules showed the absence of b1A feature. The third blue contour b3A, which represents the favorable positive charge, perhaps resulted for N<sup>+</sup> of quinolinium ring.

The inference of steric and electrostatic maps of CoMSIA is similar to that of CoMFA maps and hence analysis is given only for hydrophobic and hydrogen bond donor maps as acceptor maps are not resulted for the dataset (Table 2 and Fig. 5). One hydrophobic favorable feature, o1A, and two unfavorable features w1A and w2A were obtained where o1A is comparable to g1A of CoMFA and w1A and w2A corresponds to y2A and y3A, respectively. The o1A supports the presence of hydrophobic residues in the active site. Two donor maps, c1A and c2A which correspond to Cl and NH<sub>2</sub> groups at 7th position of the quinolinium ring were noticed. But the possibility of hydrogen bond interactions seems to be sterically restricted because of amino acid side chains orientations is not very suitable in the active site and also absence of suitable acceptor at the appropriate position.

### 3.2.2. Set B

Two steric favorable maps g1B and g2B, which corresponds to the R<sub>4</sub> position, were noticed (Fig. 4). The results of Set B are rather contrary with the results of Set A and C. May be due to the linker 4–4', which positioned the ligands differently in the active site when compared to Set A and C and the same is seen in the interactions in turn the analysis. Substitution of chloro group at 4th position of the *N*-methylanilino ring has reduced the activity for Set A and C. For example, compounds **6** (0.40 μM) to **7** (2.10 μM), **23** (3.10 μM) to **24** (5.70 μM) and **34** (56.8 μM) to **35** (147 μM) for Set A and **18** (1.40 μM) to **19** (4.80 μM) and **32** (3.50 μM) to **33** (5.70 μM) with an exception of **38** (133 μM) to **39** (57.5 μM) of Set C have followed the above mentioned trend. Quite the opposite trend has observed for Set B compounds where increase in the activity is seen for **12** (3.00 μM) to **13** (2.00 μM) and **36** (96.1 μM) to **37** (46.1 μM). The steric unfavorable y3–5B maps located near the methyl substitution at 8th position of quinolinium ring infers the low activity of **36** and **37**. The y6B map that is located inside the b2B corresponds to Cl substitution at 7th position. This is reflected in approximate 4- and 6-fold activity loss for **28** (11.4 μM) and **29** (11.4 μM) when compared to their congeners **12** (3.00 μM) and **13** (2.00 μM) whereas gain in activity is noticed for **25** (63.3 μM) and **26** (20.6 μM) from **8** (81.1 μM) and **9** (39.7 μM), respectively. The electropositive contour, b1B matches with NH<sub>2</sub> group of 7th position for **36** and **37**.

The cyan contours resulted near the NH<sub>2</sub> group of **36** and **37** suggest the possibility for hydrogen bond donation (Fig. 5). The two other cyan contours, c5B and c6B support the hydrogen bond donation particularly for **8**, **11** and **25** which holds the NH<sub>2</sub> and NH groups as donors at R<sub>4</sub> position.

### 3.2.3. Set C

The g1C and g2C contours of R<sub>4</sub> substitution suggest that the bulky groups like perhydroazepino (**16**) and pyrrolidino (**31**) may

enhance the activity (Fig. 4). The electro positive and steric bulk contours namely b1C, b2C and y2C correspond to NH<sub>2</sub> and CH<sub>3</sub> of **38** and **39**. A model missing of these two compounds has lost these three maps and further suggests that these two substitutions are not aid to the activity owing to the possibility of steric repulsions with protein at the point of interaction.

### 3.3. Docking analysis

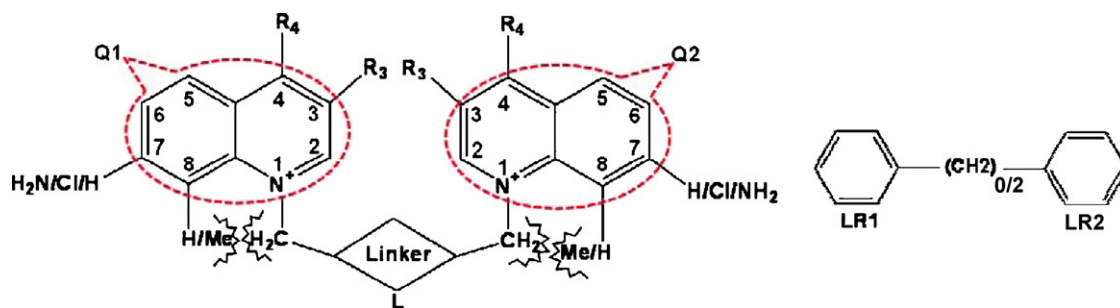
Two docking protocols, GOLD, and Glide were used to obtain the binding modes of ligands. As the two docking procedures were resulted in nearly comparable results a combined analysis of results is presented here. As mentioned earlier, two binding sites were resulted from the active site search, out of two one site (choline pocket) is of particular interest and considered as active site for the docking studies.

The crystal structure of ChoK and choline complex [28] reveals that the ammonium moiety of the choline is situated in a pocket which is created typically by seven aromatic residues, Trp420, 423, Tyr333, 354, 440 and Phe362, 435. The ethyl and phosphate groups are surrounded by Leu120, Asp306, Gln308, Asn311, Ser121 and Gly119. The N<sup>+</sup> contributes to the cation–π interactions within a distance of 4.30 Å and 5.43 Å with Trp420 and 423 residues, respectively. With tyrosine residues (354, 440, 333) shown long distance cation–π interaction within a range of 5.47–7.18 Å. The side chain NH group of Gln308 and COO<sup>−</sup> group of Asp306 and Glu349 interacts with N<sup>+</sup> with in a distance of 4.76 Å, 4.44 Å and 4.39 Å, respectively. Residues Phe362 and 435 participate in π–π and CH<sub>3</sub>–π with Tyr440 and with methyl group of choline, respectively. Besides cation–π, the residues Trp420, 423 and Tyr354, 440 have also shown CH<sub>3</sub>–π interaction with three methyl groups of ammonium ion. The ethyl chain forms hydrophobic interactions with side chain of Leu120. Residues, namely Asp306, Gln308, Asn311, Ser121 and Gly119 have shown electrostatic interactions with oxygen atoms of phosphate group. The three oxygens were participated in hydrogen bonding with side chain O and N atoms of Ser121 and Gln308, respectively and with backbone N of Leu120. These protein–substrate interactions were explicitly used to draw observations for protein and docked conformations of inhibitors. The scaffold of the dataset is classified as shown in the Scheme 3.

The Q1 is positioned in the pocket shaped by Trp423, 420 and Tyr440, 354, 333 (Fig. 6). The linker rings, LR1 and LR2, are stacked with Phe435, Tyr354 and Phe361. The R<sub>4</sub> groups facilitated the stacking interactions of Q1 either forming hydrogen bonds or through electrostatic interactions with the surrounding polar region of the active site residues. Particularly the aniline ring shows π–π stacking with Tyr333, Trp420 and His304 where the NH group comfortably participates in the hydrogen bonding with the side chain OH of Tyr440. The side chain carboxylic group of Asp306 also participates in these interactions. The Cl and NH<sub>2</sub> groups at 7th position of quinolinium ring have shown two types of binding modes either orient towards the Asp215, Asp330, Asn311, Glu332 or Tyr440 and Trp423. When R<sub>4</sub> is substituted with bulky groups like pyrrolidino or *N*-methylanilino or 4-chloro-*N*-methylanilino the Cl and NH<sub>2</sub> have shown the first orientation. The NH<sub>2</sub> group participates in hydrogen bonding with Asn311 and Asp330 side chains. However, the CH<sub>3</sub> at 8th position of quinolinium ring is not sterically suitable as it has been located in the electrostatic environment that is being created by Asp215, Asp330, Asn311, Glu332 and Arg117 residues to the first half and Arg212, 213, 215, Asp353, Thr216 and Ser355 to the second half of the molecule.

The Q2 has shown three different orientations (Fig. 6) in three distinct pockets. The Q2 ring was taken an 'S' shaped conformation to packed in between Arg117, Ser355 and shown stacking





**Scheme 3.** Pictorial representation of the dataset scaffold and the linker rings. Notations have given to the groups for better understanding the docking analysis. Steric clashes between methyl and  $-\text{CH}_2-$  have shown as half star symbols.

interactions with Phe361 which we termed as pocket1 (P1). In another mode it was positioned in such a way that it was stacked amid of Ile116 and Arg212, 213 (pocket2 – P2). The other orientation positioned the Q2 in the midst of pocket3 (P3) that is made-up of Ile116, 209, Leu116, 144, 313, Arg146 and Pro210 residues where hydrophobic interactions were noticed between Q2 ring and side chains of residues. This conformation was observed only with the linker 4'- $\text{CH}_2$ -4'' structures (**14** and **15**).

The loop between the beta sheet 1 and 2 i.e. from Ile116 to Asn122 showed the conformational deviation from ADP bound protein (*loop open*) to PCho bound protein (*loop closed*, Fig. 7) [25,28]. The conformation of the loop also decides the docking poses of ligands in the active site of two proteins (Fig. 8). However, it is difficult to conclude which is the correct binding mode until a crystal structure with known inhibitor is modeled. Because it is not sure when will the inhibitor bind to the protein before ATP binds or after? Moreover, the PCho bound protein does not comprise the ADP structure and also no loop movement is noticed. According to the hypothesis proposed by Peisach et al. [25] there would be an increase in the volume in the presence of ATP to accommodate the choline substrate. Explicitly, the loop will move up when ATP binds and creates entry for choline and it will close after choline enters. If

the inhibitor binds immediately after ATP bound to the protein the *loop open* conformation is the proper structure for docking. On the other hand, inhibitor binds prior to ATP entry then *loop close* structure is more appropriate to dock the ligands. We took both the proteins, *loop open* and *loop close*, and performed the docking. A significant variation in ligand binding is observed between these two proteins (Fig. 8). However, we consider that the protein with *loop open* conformation is rather appropriate to start the docking since it has created the entry to the choline pocket. Unless the entry is being created by ATP, either choline or inhibitors cannot enter in to the pocket. Subsequent docking studies with the *loop close* conformation have result in the potential contacts after inhibitor entered in to the pocket. When docking studies were done with *apo* proteins, 2CKO and 1NW1, no proper binding of ligands was noticed, which is also supporting the previous statement (Fig. 9). The loop conformation of 1NW1 is different from the above two and it can be considered as the initial conformation (or *apo* conformation) of the loop i.e. before any substrate (ATP or choline) binds to the protein (Fig. 9). After considering all the above points we suggest that the inhibitor competes with the choline to bind to the *loop open* structure. Furthermore, simultaneous docking studies with the *loop close* structure will provide the basic protein–ligand interactions.

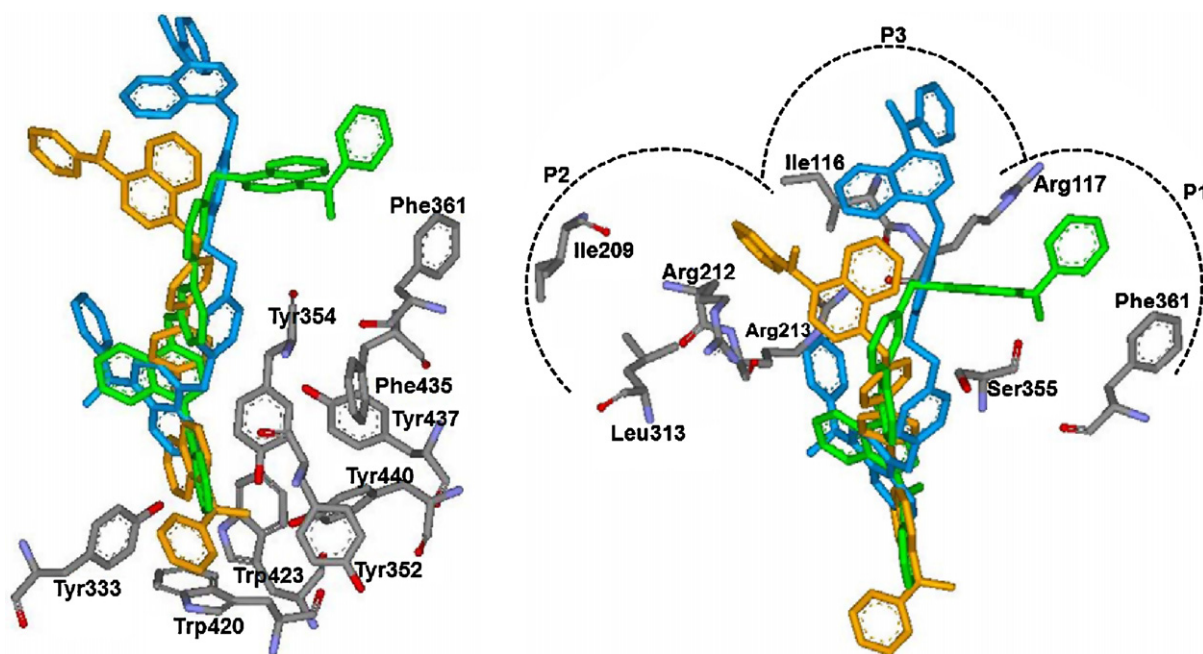


**Fig. 6.** Docked poses of ligands with different linkers **6** (green), **12** (orange) and **18** (blue) are displayed in stick rendering in the active site of choline kinase. The important active site residues which participated in interactions with Q1 ring are shown in the left side image. Residues of three pockets (P1–P3) involved in the interactions with Q2 ring are shown in right side image and residue numbers are labeled. The Q1 ring and  $\text{R}_4$  substitution have shown  $\pi$ - $\pi$  stacking with the aromatic motifs of Trp420, 423, Tyr333, 352, 354, 440, 437 and Phe361 and 435.

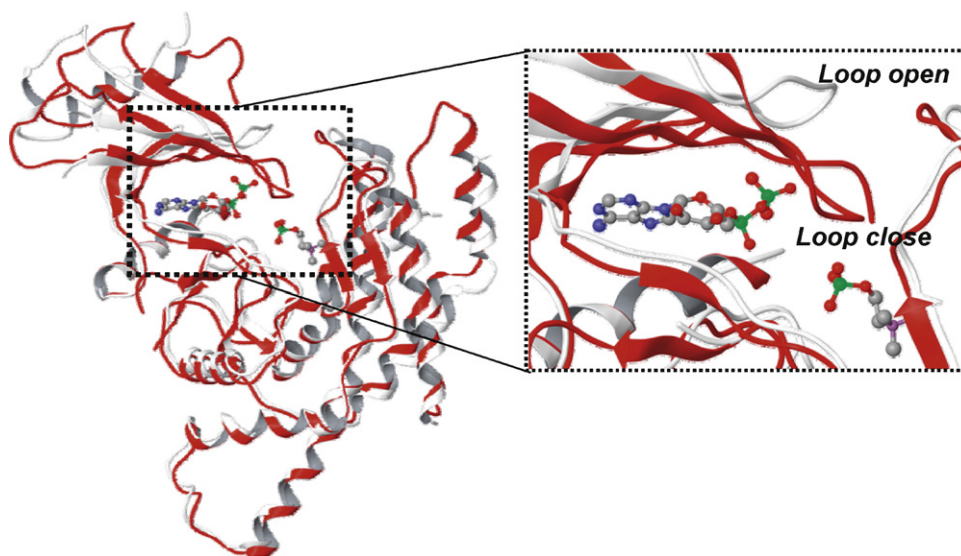


**Fig. 7.** Overlay of choline kinase proteins bound with ADP (white) and PCho (red). The loop region that is deviated (*loop open* and *loop close*) is highlighted in the square box right side. The *loop close* conformation has created relatively more space in PCho bound protein when compared to ADP bound one and also affected the way the ligands will be docked in the active site of both the proteins. The ADP and PCho have shown as ball and stick models and the protein tertiary structure is displayed as helices,  $\beta$ -sheet and turn.

Therefore, in order to obtain the complete scenario of ligand binding and its contacts with the protein active site docking was performed with both, *loop out* and *loop close*, structures.

In order to find out how compounds with three cationic heads will bind to the active site a set of 10 *tris* ligands (Table 3) were collected from Garcia et al. work [13] and docked against same proteins (*un shown data*). Expectedly, the three heads have comfortably occupied the three pockets, P1, P2 and P3 and exhibited all equivalent contacts those are mentioned above. The three cationic units have made use of the active site optimally and fasten the conformational flexibility of ligands. According to Campos et al. [20], introduction of third cationic moiety increases

the ChoK potency but in turn reduces the antiproliferative activity. Excluding this, their studies have also shown that even the *mono* cationic compounds could considerably inhibit the ChoK enzyme activity [20]. Modifying the inhibitor structure from *mono* to *bis* to *tris* has increased the ChoK inhibitory activity simultaneously [20]. This perhaps caused by increased interactions of the ligand with the active site residues by optimal exploitation of the binding pockets (P1–P3). From these results one can infer that considering the two cationic moieties does not seem to be the prerequisite for enzyme inhibition. However, they may be responsible for bringing the selectivity towards the choline kinase protein which is very important for any inhibitor or drug.

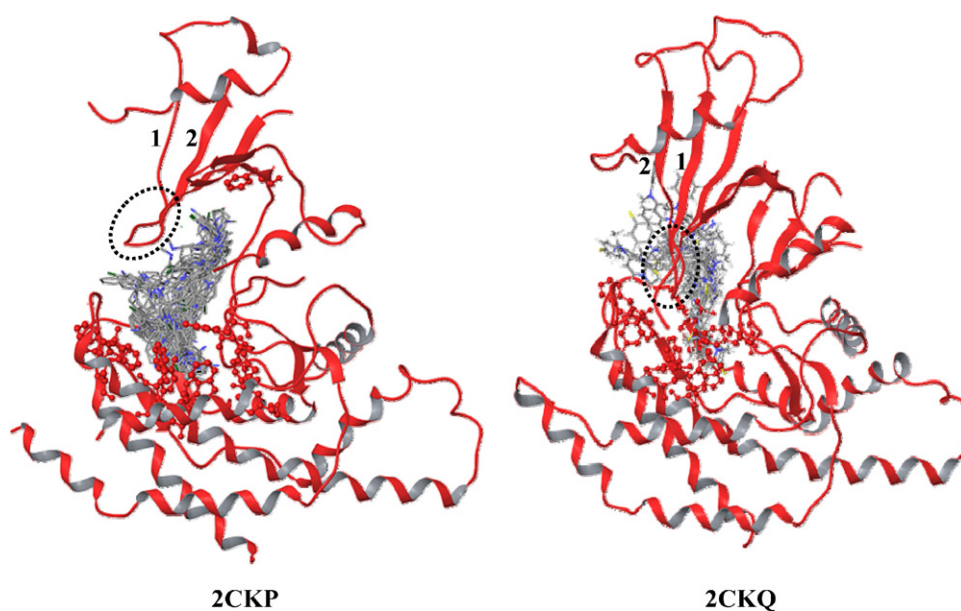


**Fig. 8.** Docked ligands are displayed in the active site of 2CKP (ADP bound) and 2CKQ (PCho bound). The difference in the binding mode of ligands in both the active sites is clearly evident because of change of loop conformation between  $\beta$ -sheet 1 and 2, highlighted in dotted circle. Important active site residues are shown as red ball and stick model.

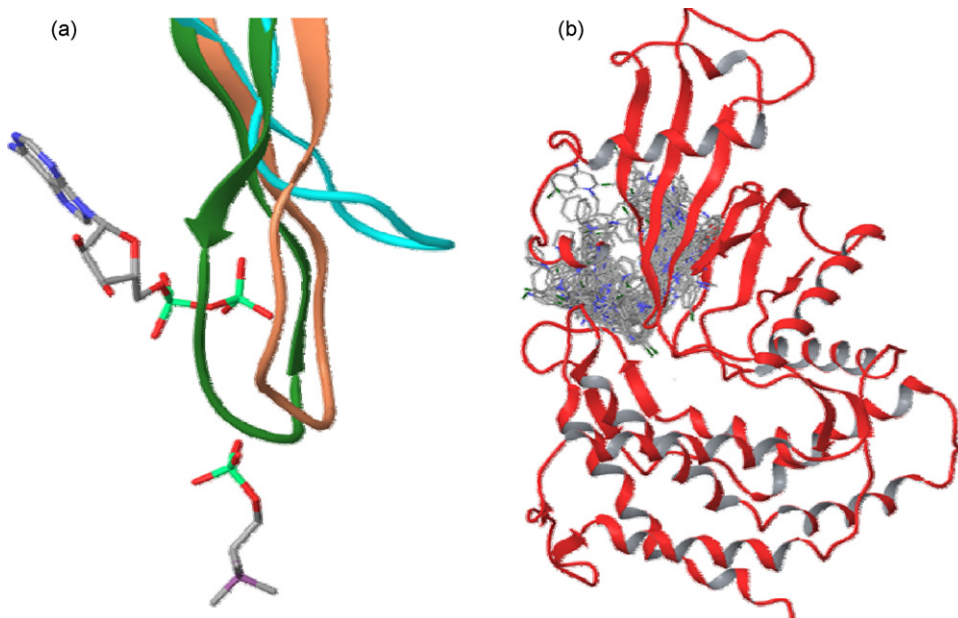
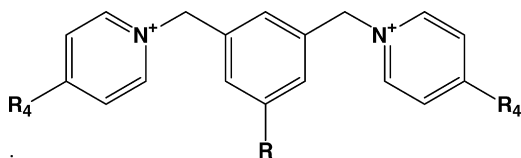


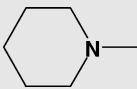
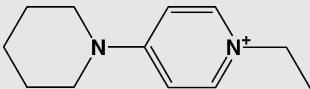
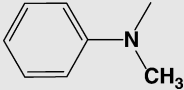
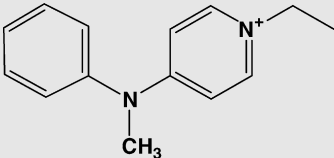
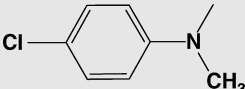
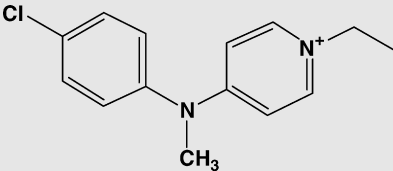
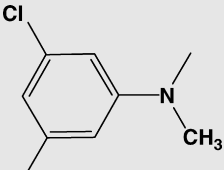
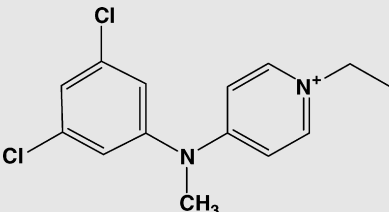
**Fig. 9.** (a) Overlay of 2CKP (ADP), 2CKQ (PCho) and 1NW1 loop regions that are displayed in cyan, orange and green colors, respectively. The ADP and PCho molecules are showed in atom color capped stick model. (b) The docked conformations of the dataset are displayed for 1NW1. All the ligands were docked outside the pocket may be due to lack of the entry to the choline pocket.

**Table 3**  
The structures of *tris*-analogs and their activities ( $IC_{50}$ ) against ChoK



Serial number	R <sub>4</sub>	R	IC <sub>50</sub>
1		H	>100
2		H	84.2
3		H	52.8
4		H	37.5
5			>100
6			7.8

Table 3 (Continued)

Serial number	R <sub>4</sub>	R	IC <sub>50</sub>
7			1.5
8			5.1
9			1.4
10			3.4

#### 4. Combine analysis of 3D-QSAR and docking results

A comparative analysis of 3D-QSAR maps and docking interactions has offered a few essential inklings that need to be considered while modifying the *bis*-quinolinium structures to augment the activity. The steric contours that are surrounded Q1 and Q2 resemble with the hydrophobic pocket created by aromatic residues and pockets P1–P3. The yellow maps (y3-5B and y2C) near the methyl substitution at 8th position suggest the possibility of steric bad contacts of the methyl group with the active site residues (Fig. 4). Even the docked conformations have supported the observation where the CH<sub>3</sub> group is found to interfere with the cation– $\pi$ – $\pi$  interactions of Q1 with Trp420, 423 and Tyr440, 354, 333. This particular substitution has introduced strain in the Q1 and Q2 rings due to steric hindrance with the N<sup>+</sup>–CH<sub>2</sub> (Scheme 3). Characteristically the Q1 complementary pocket is electronegative in nature to accommodate the positive charge of the nitrogen. The polar part of the active site residues for example, the CONH of Asn and Gln side chains as well as backbone of Gly, COOH of Asp and Glu and lastly the OH of Tyr side chain are exposed to make the active site environment more polar. The CH<sub>3</sub> of Q2 group is wrapped by polar component of Asp215, 353, Arg213, 215 and Ser355 residues. Hence, substitution of non-polar groups like CH<sub>3</sub> on Q rings is vulnerable due to lack of suitable interactions. Two donor maps, c1A and c2A correspond to Cl and NH<sub>2</sub> groups at 7th position of the quinolinium ring are resulted in CoMSIA. Though the NH<sub>2</sub> showed virtual hydrogen bonds with Asn311 and Asp330 side chains they seem to be feeble due to steric constrain. These interactions sterically restrict the Q1 orientation and in turn their participation in hydrogen bonding because of the side chains of active site residues and also absence of suitable acceptor at appropriate position. The two other cyan contours, c5B and c6B support the hydrogen bond donation particularly for those compounds which holds the NH<sub>2</sub> and NH groups as donors at R<sub>4</sub> position. There are suitable acceptors in the active site which can

enfold these groups namely Asn345, Glu349, 357, Arg146, 444, Tyr440, Ser355 and Asp215. Therefore the groups (other than chlorine) that can participate in hydrogen bonds are advantageous at R<sub>4</sub> position.

#### 5. Conclusions

The CoMFA and CoMSIA models have shown good correlation as well as predictive abilities. Addition of hydrophobic and hydrogen bond fields have considerably improved the correlation coefficient value however the predictive ability is not much improved. The docking studies revealed the potential binding modes of inhibitors. The *loop open* and *close* conformations perhaps decide the binding orientation of ligands. At the same time both the conformations need to be considered for docking to get a complete scenario of active conformations of ligands and protein–ligand contacts. The aromatic residues of the active site play a very crucial role in inhibitor interactions. Therefore, consideration of aromatic groups in inhibitor design appears to be a successful strategy. Substituents at R<sub>4</sub> position have an indirect role in stabilizing the stacking interactions of aromatic motifs by tuning the orientation of the Q ring. Further, the R<sub>4</sub> position is suitable for hydrogen bond donors. Hence, groups other than chlorine can be attempted at R<sub>4</sub> position of *bis*-quinolinium compounds. The spacer of the linker does not appear to be crucial for the activity. The linker does not show any influence on steric and electrostatic fields, but it possibly will play a crucial role in tuning the ligand–protein interactions. Substitutions, particularly steric groups at 7th and 8th positions of the Q ring are not suitable as they introduce strain in the Q ring and also intruding in the cation– $\pi$  interactions. The cycloalkylamines or aryl amino substituents are resulted as better groups for inhibitory activity than their amino or dimethyl amino derivatives may be due to increased number of contacts with the active site. Consideration of identical groups at Q1 and Q2 is not necessary



as there is no such similarity exists in the active site. Moreover, the Q1 site is fabricated mostly by aromatic residues whereas Q2 is with aliphatic residues. Lastly, having two cationic heads in the inhibitor structure is perhaps not required for the enzyme inhibition. Unlike as specified in the introduction (other choline, AChE, and non-choline proteins, PKC), the ChoK inhibitors are not binding to two specific sites instead they bind to a single site which consists of the choline entry channel. The docking poses of *tris* compounds also revealed that their exhibited activities are as a result of increased number of contacts with the active site not because of binding to different binding sites. However, presence of two or three cationic moieties will possibly bring the selectivity towards the ChoK, which is an essential feature for any inhibitor.

## Acknowledgements

PS thanks CSIR New Delhi, for a senior research fellowship. Department of Biotechnology (DBT), New Delhi is thanked for the financial support. GNS thanks DST for the support in terms of Swarnajayanthi Fellowship.

## References

- [1] R.A. Molina, R.A. González, J.C. Lical, From Ras signalling to ChoK inhibitors: a further advance in anticancer drug design, *Cancer Lett.* 206 (2004) 137–148.
- [2] S. Janardhan, P. Srivani, G.N. Sastry, Choline kinase: an important target for cancer, *Curr. Med. Chem.* 13 (2006) 1169–1186.
- [3] H.R. Alcoceba, L. Saniger, J. Campos, M.C. Nunez, F. Khaless, M.A. Gallo, A. Espinosa, J.C. Lical, Choline kinase inhibitors as a novel approach for antiproliferative drug design, *Oncogene* 15 (1997) 2289–2301.
- [4] R.A. Molina, R.A. González, V. Penalba, L. Lucas, J.C. Lical, Inhibition of ChoK is an efficient antitumor strategy for Harvey-, Kirsten-, and N-ras-transformed cells, *Biochem. Biophys. Res. Commun.* 285 (2001) 873–879.
- [5] D. Teegarden, E.J. Taparowsky, C. Kent, Altered phosphatidylcholine metabolism in C3H10T1/2 cells transfected with the Harvey-ras oncogene, *J. Biol. Chem.* 265 (1990) 6042–6047.
- [6] J.M. Campos, M.C. Nunez, S.R.M. Martin, G.J.A. Vidal, R.A. Gonzalez, M. Banez, M.A. Gallo, J.C. Lical, A. Espinosa, Quantitative structure–activity relationships for a series of symmetrical bisquaternary anticancer compounds, *Bioorg. Med. Chem.* 10 (2002) 2215–2231.
- [7] J.M. Campos, M.C. Nunez, V. Rodriguez, M.A. Gallo, A. Espinosa, QSAR of 1,10-(1,2-ethylenebisbenzyl)bis(4-substitutedpyridinium)dibromides as choline kinase inhibitors: a different approach for antiproliferative drug design, *Bioorg. Med. Chem. Lett.* 10 (2000) 767–770.
- [8] J. Campos, M.C. Nunez, V. Rodríguez, A. Entrena, M.A. Gallo, H.R. Alcoceba, F. Fernandez, J.C. Lical, A. Espinosa, LUMO energy of model compounds of bispyridinium compounds as an index for the inhibition of choline kinase, *Eur. J. Med. Chem.* 36 (2001) 215–225.
- [9] C.A. Garcia, B.M. Coronel, S.R.M. Martin, R.A. Gonzalez, A. Ramos, R.A. Molina, A. Espinosa, M.A. Gallo, J.M. Campos, J.C. Lical, Influence of the linker in bispyridinium compounds on the inhibition of human choline kinase, *J. Med. Chem.* 47 (2004) 5433–5440.
- [10] S.R. Martin, J.M. Campos, C.A. Garcia, C.O. Lopez, B.M. Coronel, R.A. Gonzalez, M.A. Gallo, J.C. Lical, A. Espinosa, Symmetrical bis-quinolinium compounds: new human choline kinase inhibitors with antiproliferative activity against the HT-29 cell line, *J. Med. Chem.* 48 (2005) 3354–3363.
- [11] J. Campos, C. Nunez, J. Diaz, M. Sanchez, M.A. Gallo, A. Espinosa, Anticancer bisquaternary heterocyclic compounds: a *ras*-ional design, *Il Farmaco* 58 (2003) 221–229.
- [12] C.A. Garcia, J. Campos, S.R. Martin, M.A. Gallo, A. Espinosa, Bispyridinium cyclophanes: novel templates for human choline kinase inhibitors, *J. Med. Chem.* 46 (2003) 3754–3757.
- [13] (a) C.A. Garcia, A. Entrena, J.M. Campos, R.S. Martin, M.A. Gallo, A. Espinosa, Towards a model for the inhibition of choline kinase by a new type of inhibitor, *Eur. J. Med. Chem.* 40 (2005) 315–319; (b) C.A. Garcia, J. Campos, R.M. Sanchez, R.A. Gonzalez, J.C. Lical, M.A. Gallo, A. Espinosa, Choline kinase inhibitory effect and antiproliferative activity of new 1,1',1''-(benzene-1,3,5-trimethylene)tris(4-[disubstituted]amino)pyridinium} tribromides, *Eur. J. Med. Chem.* 38 (2003) 109–116.
- [14] G.B. Ansell, S.G. Spanner, The inhibition of brain choline kinase by hernicholinium-3, *J. Neurochem.* 22 (1974) 1153–1155.
- [15] A. Cuadrado, A. Carnero, F. Dolfi, B. Jimenez, J.C. Lical, Phosphorylcholine: a novel second messenger essential for mitogenic activity of growth factors, *Oncogene* 8 (1993) 2959–2968.
- [16] K.S. Crilly, M. Tomono, Z. Kiss, The choline kinase inhibitor hemicholinium-3 can inhibit mitogen-induced DNA synthesis independent of its effect on phosphocholine formation, *Arch. Biochem. Biophys.* 352 (1998) 137–143.
- [17] B. Jimenez, L. del Peso, S. Montaner, P. Esteve, J.C. Lical, Generation of phosphorylcholine as an essential event in the activation of Raf-1 and MAP-kinases in growth factors-induced mitogenic stimulation, *J. Cell. Biochem.* 57 (1995) 141–149.
- [18] H.R. Alcoceba, F. Fernandez, J.C. Lical, *In vivo* antitumor activity of choline kinase inhibitors: a novel target for anticancer drug discovery, *Cancer Res.* 59 (1999) 3112–3118.
- [19] A.S. Reddy, P.S. Priyadarshini, P.P. Kumar, H.N. Pradeep, G.N. Sastry, Virtual screening in drug discovery—a computational perspective, *Curr. Prot. Pep. Sci.* 8 (2007) 329–351.
- [20] J. Campos, M.C. Nunez, C.A. Garcia, R.M.S. Martin, R.H. Alcoceba, A.R. Gonzalez, J.C. Lical, M.A. Gallo, A. Espinosa, QSAR-derived choline kinase inhibitors: how rational can antiproliferative drug design be? *Curr. Med. Chem.* 10 (2003) 1095–1112.
- [21] (a) A.S. Reddy, G.N. Sastry, Cation [M = H<sup>+</sup>, Li<sup>+</sup>, Na<sup>+</sup>, K<sup>+</sup>, Ca<sup>2+</sup>, Mg<sup>2+</sup>, NH<sub>4</sub><sup>+</sup>, and NMe<sub>4</sub><sup>+</sup>] interactions with the aromatic motifs of naturally occurring amino acids: a theoretical study, *J. Phys. Chem. A* 109 (2005) 8893–8903; (b) A.S. Reddy, G.M. Sastry, G.N. Sastry, Cation—aromatic database (CAD), *Proteins: Struct. Funct. Bioinform.* 67 (2007) 1179–1184.
- [22] (a) A.S. Reddy, D. Vijay, G.M. Sastry, G.N. Sastry, From subtle to substantial: role of metal ions on  $\pi$ - $\pi$  interactions, *J. Phys. Chem. B* 110 (2006) 2479–2481; (b) D. Vijay, H. Zipse, G.N. Sastry, On the cooperativity of cation- $\pi$  and hydrogen bonding interactions, *J. Phys. Chem. B* 112 (2008) 8863–8867.
- [23] (a) Q. Xie, Y. Tang, W. Li, X. Wang, Z. Qiu, Investigation of the binding mode of (–)-meptazinol and bis-meptazinol derivatives on acetylcholinesterase using a molecular docking method, *J. Mol. Model.* 12 (2006) 390–397; (b) M.L. Bolognesi, A. Cavalli, L. Valgimigli, M. Bartolini, M. Rosini, V. Andrisano, M. Recanatini, C. Melchiorre, Multi-target-directed drug design strategy: From a dual binding site acetylcholinesterase inhibitor to a trifunctional compound against Alzheimer's disease, *J. Med. Chem.* 50 (2007) 6446–6449; (c) Q. Xie, H. Wang, Z. Xia, M. Lu, W. Zhang, X. Wang, W. Fu, Y. Tang, W. Sheng, W. Li, W. Zhou, X. Zhu, Z. Qiu, H. Chen, Bis-(–)-nor-meptazinols as novel nanomolar cholinesterase inhibitors with high inhibitory potency on amyloid- $\beta$  aggregation, *J. Med. Chem.* 51 (2008) 2027–2036.
- [24] D. Qin, R. Sullivan, W.F. Berkowitz, R. Bittman, S.A. Rotenberg, Inhibition of protein kinase C $\alpha$  by dequalinium analogues: dependence on linker length and geometry, *J. Med. Chem.* 43 (2000) 1413–1417.
- [25] D. Peisach, P. Gee, C. Kent, Z. Xu, The crystal structure of choline kinase reveals a eukaryotic protein kinase fold, *Structure* 11 (2003) 703–713.
- [26] (a) S. Janardhan, P. Srivani, G.N. Sastry, 2D and 3D quantitative structure–activity relationship studies on a series of bis-pyridinium compounds as choline kinase inhibitors, *QSAR Comb. Sci.* 25 (2006) 860–872; (b) P. Srivani, K. Kiran, G.N. Sastry, Understanding the structural requirements of triarylethane analogues towards PDE IV inhibitors: a molecular modeling study, *Ind. J. Chem. A* 45A (2006) 68–76; (c) P. Srivani, E. Srinivas, R. Raghu, G.N. Sastry, Molecular modeling studies of pyridopyrimidine derivatives—potential phosphodiesterase 5 inhibitors, *J. Mol. Graph. Model.* 26 (2007) 378–390; (d) R.G. Kulkarni, P. Srivani, G. Achaiah, G.N. Sastry, Strategies to design of pyrazolyl urea derivatives for p38 kinase inhibition: a molecular modeling study, *J. Comp. Aid. Mol. Design.* 25 (2007) 155–166.
- [27] C. Yuan, C. Kent, Identification of critical residues of choline kinase A2 from *Caenorhabditis elegans*, *J. Biol. Chem.* 279 (2004) 17801–17809.
- [28] E. Malito, N. Sekulic, W.C.S. Too, M. Konrad, A. Lavie, Elucidation of human choline kinase crystal structures in complex with the products ADP or phosphocholine, *J. Mol. Biol.* 364 (2006) 136–151.
- [29] SYBYL 6.9. Molecular Modeling Software, Tripos Inc. (1999) Hanley Road, St. Louis, MO 63144.
- [30] GOLD, version 2.2, Cambridge Crystallographic Data Centre, Cambridge, U.K.
- [31] Glide, version 4.5, Schrödinger, LLC, New York, NY, 2007.
- [32] G. Klebe, U. Abraham, T. Mietzner, Molecular similarity indices in a comparative analysis (CoMSIA) of drug molecules to correlate and predict their biological activity, *J. Med. Chem.* 37 (1994) 4130–4146.
- [33] R. Bohacek, S. McMartin, Definition and display of steric, hydrophobic, and hydrogen bonding properties of ligand binding sites in proteins using Lee and Richards accessible surface: validation of a high-resolution graphical tool for drug design, *J. Med. Chem.* 35 (1992) 1671–1684.
- [34] V.N. Viswanadhan, A.K. Ghose, R. Revenkar, R.N. Robins, Atomic physicochemical parameters for three dimensional structure directed quantitative structure–activity relationships. 4. Additional parameters for hydrophobic and dispersive interactions and their application for an automated superposition of certain naturally occurring nucleoside antibiotics, *J. Chem. Inf. Comput. Sci.* 29 (1989) 163–172.
- [35] R.D. Cramer, D.E. Patterson, J.D. Bunce, Comparative molecular field analysis (CoMFA). 1. Effect of shape on binding of steroids to carrier proteins, *J. Am. Chem. Soc.* 110 (1988) 5959–5967.
- [36] R.D. Cramer, J.D. Bunce, D.E. Patterson, Crossvalidation, bootstrapping, and partial least squares compared with multiple regression in conventional QSAR studies, *Quant. Struct.-Act. Relat.* 7 (1988) 18–25.
- [37] P. Diaconis, B. Efron, Computer intensive methods in statistics, *Sci. Am.* 248 (1983) 116–130.
- [38] J.G. Topliss, R.P. Edwards, Chance factors in studies of quantitative structure–activity relationships, *J. Med. Chem.* 22 (1979) 1238–1244.
- [39] C.M.W. Ho, G.R. Marshall, CAVITY SEARCH: An algorithm for the isolation and display of cavity-like binding regions, *J. Comput. Aided. Mol. Design.* 4 (1990) 337–354.